

Majorana tunneling in a one-dimensional wire with non-Hermitian double quantum dots

Peng-Bin Niu(牛鹏斌) and Hong-Gang Luo(罗洪刚)
Citation: Chin. Phys. B, 2024, 33 (**1**): 017403. DOI: 10.1088/1674-1056/ad0145
Journal homepage: http://cpb.iphy.ac.cn; http://iopscience.iop.org/cpb

What follows is a list of articles you may be interested in

A ten-fold coordinated high-pressure structure in hafnium dihydrogen with increasing superconducting transition temperature induced by enhancive pressure

Yan-Qi Wang(王妍琪), Chuan-Zhao Zhang(张传钊), Jin-Quan Zhang(张金权), Song Li(李松), Meng Ju(巨濛), Wei-Guo Sun(孙伟国), Xi-Long Dou(豆喜龙), and Yuan-Yuan Jin(金园园)
Chin. Phys. B, 2023, 32 (**9**): 097402. DOI: 10.1088/1674-1056/acc934

Anisotropic superconducting properties of $FeSe_{0.5}Te_{0.5}$ single crystals

Jia-Ming Zhao(赵佳铭) and Zhi-He Wang(王智河)
Chin. Phys. B, 2022, 31 (**9**): 097402. DOI: 10.1088/1674-1056/ac5610

Negative tunnel magnetoresistance in a quantum dot induced by interplay of a Majorana fermion and thermal-driven ferromagnetic leads

Peng-Bin Niu(牛鹏斌), Bo-Xiang Cui(崔博翔), and Hong-Gang Luo(罗洪刚)
Chin. Phys. B, 2021, 30 (**9**): 097401. DOI: 10.1088/1674-1056/abf10b

Evidence for topological superconductivity: Topological edge states in Bi_2Te_3/FeTe heterostructure

Bin Guo(郭斌), Kai-Ge Shi(师凯歌), Hai-Lang Qin(秦海浪), Liang Zhou(周良), Wei-Qiang Chen(陈伟强), Fei Ye(叶飞), Jia-Wei Mei(梅佳伟), Hong-Tao He(何洪涛), Tian-Luo Pan(潘天洛), Gan Wang(王干)
Chin. Phys. B, 2020, 29 (**9**): 097403. DOI: 10.1088/1674-1056/abaf9c

Chiral p-wave pairing of ultracold fermionic atoms due to a quadratic band touching

Hai-Xiao Wang(王海啸), Zi-Heng Liu(刘子衡), Jian-Hua Jiang(蒋建华)
Chin. Phys. B, 2018, 27 (**2**): 027402. DOI: 10.1088/1674-1056/27/2/027402

Majorana tunneling in a one-dimensional wire with non-Hermitian double quantum dots

Peng-Bin Niu(牛鹏斌)[1,†] and Hong-Gang Luo(罗洪刚)[2,3]

[1] *Institute of Solid State Physics, Shanxi Datong University, and Shanxi Provincial Key Laboratory of Microstructural Electromagnetic Functional Materials, Datong* 037009, *China*
[2] *School of Physical Science and Technology, Lanzhou University, Lanzhou* 730000, *China*
[3] *Beijing Computational Science Research Center, Beijing* 100084, *China*

(Received 7 July 2023; revised manuscript received 6 October 2023; accepted manuscript online 9 October 2023)

The combination of non-Hermitian physics and Majorana fermions can give rise to new effects in quantum transport systems. In this work, we investigate the interplay of PT-symmetric complex potentials, Majorana tunneling and interdot tunneling in a non-Hermitian double quantum dots system. It is found that in the weak-coupling regime the Majorana tunneling has pronounced effects on the transport properties of such a system, manifested as splitting of the single peak into three and a reduced $1/4$ peak in the transmission function. In the presence of the PT-symmetric complex potentials and interdot tunneling, the 1/4 central peak is robust against them, while the two side peaks are tuned by them. The interdot tunneling only induces asymmetry, instead of moving the conductance peak, due to the robustness of the Majorana modes. There is an exceptional point induced by the union of Majorana tunneling and interdot tunneling. With increased PT-symmetric complex potentials, the two side peaks will move towards each other. When the exceptional point is passed through, these two side peaks will disappear. In the strong-coupling regime, the Majorana fermion induces a $1/4$ conductance dip instead of the three-peak structure. PT-symmetric complex potentials induce two conductance dips pinned at the exceptional point. These effects should be accessible in experiments.

Keywords: Majorana fermion, non-Hermitian quantum dot, parity–time symmetry, exceptional point

PACS: 74.25.F–, 73.21.La, 81.07.Gf, 73.23.–b **DOI:** 10.1088/1674-1056/ad0145

1. Introduction

In quantum mechanics, there is a fundamental postulation: a physical observable must be expressed by a Hermitian operator, which ensures the eigenvalues of the operator are real and measurable. A generalization to this postulation can be made by considering non-Hermitian Hamiltonians with parity–time (PT) symmetry.[1–4] These non-Hermitian Hamiltonians can exhibit a real spectrum and exceptional points,[5–7] where eigenvalues are degenerate at certain values of non-Hermitian parameters. Physically, non-Hermitian Hamiltonians are usually used to describe open quantum systems,[6,8–11] which experience gain and loss of energy due to coupling to the environment. Non-Hermitian Hamiltonians can also be realized in fermionic systems,[12,13] where theoretical works have demonstrated that non-Hermitian topological phases can be realized.

In this work, we consider the transport properties of a hybrid fermionic system consisting of Majorana fermions and non-Hermitian double quantum dots. In fact, many works discuss Hermitian quantum dots interacting with Majorana fermions.[14–27] However, here we focus on the interplay of PT-symmetric complex potentials, Majorana tunneling and interdot tunneling in a non-Hermitian quantum dot system. We expect that the combination of PT-symmetric complex potentials, Majorana tunneling and interdot tunneling would induce an exceptional point that has not been discussed before. Then we explore the transport properties of this system. Some interesting results are found. For instance, we find that their joint effects mainly are splitting, a $1/4$ conductance peak, asymmetry, and an exceptional point. More specifically, Majorana tunneling would split the single peak into three and manifest itself as a reduced $1/4$ central peak. There is an exceptional point induced by the union of Majorana tunneling and interdot tunneling. When Majorana tunneling appears, the antiresonance induced by PT-symmetric complex potentials would disappear. The interdot tunneling would induce asymmetry, instead of moving the conductance peak. These effects are revealed in the transmission function. The model considered in this work is exactly solvable. In order to find analytical results for the retarded Green's functions contained in the transmission function, we use the equation-of-motion method.

This paper is organized as follows. In Section 2 we present the model of the studied system, define the transmission function and describe the method used in calculations. To gain an intuitive understanding of the transport properties, we present the numerical results in Section 3. Finally, the paper is summarized in Section 4.

2. Model and method

We study the quantum transport of two parallel quantum dots coupled to each other through hopping, with each

†Corresponding author. E-mail: niupengbin@163.com

© 2024 Chinese Physical Society and IOP Publishing Ltd

of them side-attached to a topological superconductor, which supports Majorana fermions at the endpoint. The system is placed between two semi-infinite wires, as as illustrated in Fig. 1. We consider a poor man's Majorana fermions, i.e., only one Majorana fermion at the end of the superconductor wire is considered.[28–30] The whole system can be modeled by the Hamiltonian[29,31–34] $H = H_{\rm wires} + H_{\rm T} + H_{\rm c}$. The first term stands for the left and right semi-infinite wires, which are modeled as hopping of noninteracting quasiparticles in a line

$$H_{\rm wires} = \sum_{\alpha}\sum_{j=1}^{\infty}\left(t_0 c_{\alpha j}^{\dagger} c_{\alpha j+1} + {\rm H.c.}\right), \tag{1}$$

where $\alpha = {\rm L,R}$ denotes the left or right wire, with $c_{\alpha j}^{\dagger}$ the creation operator for an electron in wire α at site j. Here t_0 is the hopping amplitude between the nearest sites. The second term describes the tunneling coupling between the dots and the wires,

$$H_{\rm T} = \sum_{\alpha i}\left(v_{\alpha i} c_{\alpha 1}^{\dagger} d_i + {\rm H.c.}\right), \tag{2}$$

where $i = 1,2$ is the index for the first or second quantum dot. $v_{\alpha i}$ is the tunneling amplitude between the ith dot and wire α. d_i is the annihilation operator for the ith dot. It is worth mentioning that, in normal metallic leads, the free electrons in the leads are tunnel-coupled with a quantum dot. Thus the metallic leads are three-dimensional in real space. However, compared with metallic leads,[35] the one-dimensional wire combined with the model in this work yields different transport behaviors in the weak- and strong-coupling regimes. We will show this in the discussion in Section 3. The last term of the total Hamiltonian models the hybrid subsystem consisting of two quantum dots and two Majorana fermions, which can be described by the following Hamiltonian:

$$\begin{aligned} H_{\rm c} =\ & \varepsilon_1 n_1 + \varepsilon_2 n_2 + t_{\rm c}\left(d_1^{\dagger} d_2 + d_2^{\dagger} d_1\right) \\ & + \lambda(d_1 - d_1^{\dagger})\gamma_1 + \lambda(d_2 - d_2^{\dagger})\gamma_2, \end{aligned} \tag{3}$$

where ε_i is the ith dot's energy level. $n_1 = d_1^{\dagger} d_1$ and $n_2 = d_2^{\dagger} d_2$ are the number operators for each dot. $t_{\rm c}$ is the hopping amplitude between double quantum dots. Following Refs. [31,32], we introduce PT-symmetric complex potentials into two quantum dots by considering $\varepsilon_1 = \varepsilon + {\rm i}\beta$ and $\varepsilon_1 = \varepsilon - {\rm i}\beta$. ε is a single energy level, and it can be tuned by the gate voltage. For simplicity, we will consider the case of on-resonance $(\varepsilon = 0)$ in the following discussion. When ε_i is complex, the Hamiltonian becomes non-Hermitian. Note that in practice $\pm{\rm i}\beta$ represents the physical gain and loss during the interactions between the environment and the dots.[36] The Majorana operators, γ_1 and γ_2, describe the Majorana zero modes side-coupled with the quantum dot. λ stands for the parameter of tunnel coupling between the dot and Majorana zero mode. A Hamiltonian is said to be PT-symmetric if it is invariant under the combination of parity and time reversal transformations. With respect to our model considered here, the effect of parity transformation is P: $c_{{\rm L}j} \to c_{{\rm R}j}$, $d_1 \to d_2$, $\gamma_1 \to \gamma_2$, and the effect of time reversal transformation is T: ${\rm i} \to -{\rm i}$. It is easy to check that the total Hamiltonian in this work preserves PT symmetry, under the condition of $v_{\alpha i} = v_{\alpha' i'} = v$. It is worth discussing the experimental realization of this system. In fact, the PT-symmetric complex potentials are easy to realize by coupling quantum point contacts with the quantum dots.[13] On the other hand, although theorists have predicted the existence of Majorana fermions in topological superconductors, it is still challenging to provide convincing experiments. Fortunately, there is accumulating positive evidence that Majorana zero modes are being realized.[37,38]

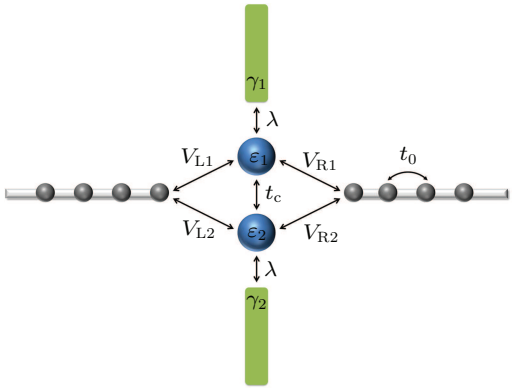


Fig. 1. Schematic representation of the Majorana–quantum-dot hybrid system, which is placed between two semi-infinite wires. The system is formed by the coupling between two quantum dots, and each dot is side-coupled to a Majorana zero-energy mode.

The Majorana operators fulfill the algebraic relation $\{\gamma_i, \gamma_j\} = 2\delta_{ij}$, and they can be expressed in terms of fermion operators as $\gamma_1 = f_1^{\dagger} + f_1$, $\gamma_2 = f_2^{\dagger} + f_2$. With these operators, the Hamiltonian in Eq. (3) becomes

$$\begin{aligned} H_{\rm c} =\ & \varepsilon_1 n_1 + \varepsilon_2 n_2 + t_{\rm c}\left(d_1^{\dagger} d_2 + d_2^{\dagger} d_1\right) \\ & + \lambda d_1(f_1^{\dagger} + f_1) + \lambda(f_1^{\dagger} + f_1) d_1^{\dagger} \\ & + \lambda d_2(f_2^{\dagger} + f_2) + \lambda(f_2^{\dagger} + f_2) d_2^{\dagger}. \end{aligned} \tag{4}$$

We expect the model considered in this work would introduce the appearance of exceptional points. Hence the eigenenergies of the central Hamiltonian decoupled from the wires (denoted as $H_{\rm c}$) should be investigated. In the basis states $\{|0\rangle, |1\rangle\}_{\rm Dot1} \otimes \{|0\rangle, |1\rangle\}_{\rm Majorana1} \otimes \{|0\rangle, |1\rangle\}_{\rm Dot2} \otimes \{|0\rangle, |1\rangle\}_{\rm Majorana2}$, the Hamiltonian is not diagonal. However, by calculation it is easy to know that these states are divided into two groups, i.e., two subspaces. In each subspace the matrix of the Hamiltonian $H_{\rm c}$ is the same. With the matrix, we obtain the eigenenergies as follows:

$$E = 0, \pm\sqrt{t_{\rm c}^2 + (2\lambda)^2 - \beta^2}, \tag{5}$$

which possess an exceptional point when $\beta = \sqrt{t_{\rm c}^2 + (2\lambda)^2}$.

In this work, we would like to use Green's function method to carry out the calculation. Therefore, the transmission function can be expressed as[39]

$$T(\omega) = \mathrm{Tr}\left[\boldsymbol{G}^{\mathrm{a}}\boldsymbol{\Gamma}^{\mathrm{R}}\boldsymbol{G}^{\mathrm{r}}\boldsymbol{\Gamma}^{\mathrm{L}}\right]. \tag{6}$$

where $\boldsymbol{G}^{\mathrm{r}}$ is the retarded Green's function in the frequency domain. It is composed of a 2×2 matrix and its elements are given by $G^{\mathrm{r}}_{ij}(\omega) = \langle\langle d_i|d_j^{\dagger}\rangle\rangle$, where the index $i,j = 1,2$. $\boldsymbol{G}^{\mathrm{a}}$ is the advanced Green's function, which can be obtained by taking the complex conjugate of $\boldsymbol{G}^{\mathrm{r}}$. $\boldsymbol{\Gamma}^{\alpha} = \Sigma_{\alpha} - \Sigma_{\alpha}^{\dagger}$ denotes the tunnel coupling between wire α and the dots. Σ_{α} is the self-energy matrix, which will be given below.

In order to obtain $\boldsymbol{G}^{\mathrm{r}}$, we use the standard equation of motion (EOM) technique,[40,41] $\omega\langle\langle A|B\rangle\rangle^{\mathrm{r}} = \langle\{A,B\}\rangle + \langle\langle[A,H]|B\rangle\rangle^{\mathrm{r}}$, where A and B are arbitrary operators. For example, the equation of motion of $\langle\langle d_1|d_1^{\dagger}\rangle\rangle$ generates

$$\begin{aligned}&(\omega-\varepsilon_1)\langle\langle d_1|d_1^{\dagger}\rangle\rangle\\ &= 1+\sum_{\alpha} v_{\alpha 1}^{*}\langle\langle c_{\alpha 1}|d_1^{\dagger}\rangle\rangle - \lambda\langle\langle f_1|d_1^{\dagger}\rangle\rangle - \lambda\langle\langle f_1^{\dagger}|d_1^{\dagger}\rangle\rangle.\end{aligned} \tag{7}$$

Due to the uniform inter-site coupling in wire α, the EOM of $\langle\langle c_{\alpha 1}|d_1^{\dagger}\rangle\rangle$ can be written out as $\sum_{\alpha} v_{\alpha 1}^{*}\langle\langle c_{\alpha 1}|d_1^{\dagger}\rangle\rangle = \Sigma_{11}\langle\langle d_1|d_1^{\dagger}\rangle\rangle + \Sigma_{12}\langle\langle d_2|d_1^{\dagger}\rangle\rangle$. The self-energy is defined as $\Sigma_{ij} = \sum_{\alpha} v_{\alpha i}^{*} v_{\alpha j} g_0$, with $g_0 = \omega/(2t_0^2) - \mathrm{i}\sqrt{4t_0^2-\omega^2}/(2t_0^2)$.[36,42] As usual, it is seen from Eq. (7) that the correlation function $\langle\langle d_1|d_1^{\dagger}\rangle\rangle$ generates new ones. These correlation functions will close naturally because the model in our work is exactly solvable. One will get a set of eight Green's functions: $\langle\langle d_1|d_1^{\dagger}\rangle\rangle$, $\langle\langle d_2|d_1^{\dagger}\rangle\rangle$, $\langle\langle d_1^{\dagger}|d_1^{\dagger}\rangle\rangle$, $\langle\langle d_2^{\dagger}|d_1^{\dagger}\rangle\rangle$, $\langle\langle f_1|d_1^{\dagger}\rangle\rangle$, $\langle\langle f_1^{\dagger}|d_1^{\dagger}\rangle\rangle$, $\langle\langle f_2|d_1^{\dagger}\rangle\rangle$, $\langle\langle f_2^{\dagger}|d_1^{\dagger}\rangle\rangle$. For conciseness, the EOM of these Green's functions will not be given here. Instead, we give the final result for the retarded Green's function

$$\boldsymbol{M}\begin{bmatrix}\langle\langle d_1|d_i^{\dagger}\rangle\rangle\\ \langle\langle d_1^{\dagger}|d_i^{\dagger}\rangle\rangle\\ \langle\langle d_2|d_i^{\dagger}\rangle\rangle\\ \langle\langle d_2^{\dagger}|d_i^{\dagger}\rangle\rangle\end{bmatrix} = \begin{bmatrix}\delta_{1,i}\\ 0\\ \delta_{2,i}\\ 0\end{bmatrix}, \tag{8}$$

where $\delta_{1,i}$ is the Kronecker delta and $i = 1,2$. The matrix reads

$$\boldsymbol{M} = \begin{bmatrix} \omega-\varepsilon_1-\frac{2\lambda^2}{\omega}-\Sigma_{11} & \frac{2\lambda^2}{\omega} & -t_{\mathrm{c}}-\Sigma_{12} & 0\\ \frac{2\lambda^2}{\omega} & \omega+\varepsilon_1-\frac{2\lambda^2}{\omega}-\Sigma_{11} & 0 & t_{\mathrm{c}}-\Sigma_{12}\\ -t_{\mathrm{c}}-\Sigma_{12} & 0 & \omega-\varepsilon_2-\frac{2\lambda^2}{\omega}-\Sigma_{22} & \frac{2\lambda^2}{\omega}\\ 0 & t_{\mathrm{c}}-\Sigma_{12} & \frac{2\lambda^2}{\omega} & \omega+\varepsilon_2-\frac{2\lambda^2}{\omega}-\Sigma_{22}\end{bmatrix}. \tag{9}$$

By using Cramer's rule, equation (8) is solved and the analytical results for elements of $\boldsymbol{G}^{\mathrm{r}}$ are obtained as

$$\langle\langle d_1|d_1^{\dagger}\rangle\rangle = \frac{1}{W_1 + \frac{2\lambda^2}{\omega}\frac{A_{12}}{A_{11}} + (-t_{\mathrm{c}}-\Sigma_{12})\frac{A_{13}}{A_{11}}}, \tag{10}$$

$$\langle\langle d_2|d_1^{\dagger}\rangle\rangle = \frac{1}{W_1\frac{A_{11}}{A_{13}} + \frac{2\lambda^2}{\omega}\frac{A_{12}}{A_{13}} + (-t_{\mathrm{c}}-\Sigma_{12})}, \tag{11}$$

$$\langle\langle d_1|d_2^{\dagger}\rangle\rangle = \langle\langle d_2|d_1^{\dagger}\rangle\rangle, \tag{12}$$

$$\langle\langle d_2|d_2^{\dagger}\rangle\rangle = \frac{1}{W_2 + \frac{2\lambda^2}{\omega}\frac{A_{34}}{A_{33}} + (-t_{\mathrm{c}}-\Sigma_{21})\frac{A_{31}}{A_{33}}}, \tag{13}$$

where A_{11}, A_{12}, A_{13}, A_{33}, and A_{34} are algebraic cofactors of the matrix in Eq. (9). $W_{1,2}$ are defined as $W_{n=1,2} = \omega - \varepsilon_n - 2\lambda^2/\omega - \Sigma_{nn}$ for brevity. Equations (10)–(13) for $\boldsymbol{G}^{\mathrm{r}}$ represent one of the main results in this work.

3. Results and discussion

In this section, we investigate the quantum transport properties induced by the interplay of PT-symmetric complex potentials, Majorana tunneling and interdot tunneling in the system. In numerical calculations, we take $t_0 = 1$, i.e., it is taken as the unit of energy. We discuss transport in the weak-coupling regime ($v \ll t_0$) first, and take dot–wire coupling as $v = 0.2$, without loss of generality.

As a beginning, in Fig. 2 we show the transport properties caused by interdot tunneling (t_{c}), Majorana tunneling (λ) or PT-symmetric complex potentials (β) separately. In the case of $t_{\mathrm{c}} = 0$, $\lambda = 0$, and $\beta = 0$, it is seen in Fig. 2(a) that the transmission function shows a Breit–Wigner lineshape whose peak reaches $T(\omega) = 1$ and is centered at $\omega = 0$. When interdot tunneling is nonzero ($t_{\mathrm{c}} \neq 0$), the peak is shifted to $\omega = t_{\mathrm{c}}$. In the case of $\lambda \neq 0$, it is seen that the effect of Majorana tunneling is to split the single peak into three. These peaks are located at $\omega = 0, \pm 2\lambda$. Another characteristic of the Majorana fermion in this model is that the central peak at $\omega = 0$ is reduced to $1/4$, as seen in Fig. 2(b). In Fig. 2(c), when $\beta \neq 0$, an antiresonance appears at $\omega = 0$, which is a typical phenomenon induced by PT-symmetric complex potentials. With β increasing, the height of peaks in transmission function is usually suppressed.

In Fig. 2 the separate effects induced by interdot tunneling (t_{c}), Majorana tunneling (λ) or PT-symmetric complex potentials (β) have been considered. We now consider their pairwise joint effects. In Fig. 3(a), the joint effect of t_{c} and λ is investigated. One can readily find that the effect of interdot tunneling is to make the three-peak structure asymmetric. But the positions of these three peaks are pinned with different t_{c}, which is a demonstration of the Majorana fermion's robustness. In the meantime, one can see that the $1/4$ central peak maintains itself, i.e., it is immune to the interdot tunneling. In

Fig. 3(b), the joint effect of λ and β is examined. The PT-symmetric complex potentials tune the two side peaks, while the $1/4$ central peak is still robust. This behavior is visualized by the curve of $\beta = 0.5$. With increasing β, the two side peaks move towards $\omega = 0$. They meet each other and merge when the exceptional point appears, i.e., when $\beta = 2\lambda$, which is seen in the curve of $\beta = 1$. When $\beta > 2\lambda$, the two side peaks disappear and the central $1/4$ peak is left alone, as seen in the curve of $\beta = 1.5$. In Fig. 3(c), the interplay of t_c and β is discussed. When β is small, the PT-symmetric complex potentials induce an antiresonance and two resonance peaks at $\omega = \pm t_c$. This is seen in the curve of $\beta = 0.1$. With increasing β, the position of the antiresonance will not change, but the resonance peaks at $\omega = \pm t_c$ will move towards each other. These two resonance peaks also merge when the exceptional point is reached, i.e., when $\beta = t_c$. This behavior is seen in the curve of $\beta = 0.2$. When $\beta > t_c$, these two resonance peaks also disappear and the resonance peak at $\omega = t_c$ is restored; its magnitude will be suppressed with increasing β. This is seen in the curve of $\beta = 0.3$. Comparing Figs. 2(c), 3(b) and 3(c), a conclusion is drawn: the antiresonance induced by PT-symmetric complex potentials appears only when $\lambda \neq 0$. Thus one can predict that the joint effects induced by PT-symmetric complex potentials, Majorana tunneling and interdot tunneling will be similar to those in Fig. 3(b). Meanwhile, asymmetry is to appear there.

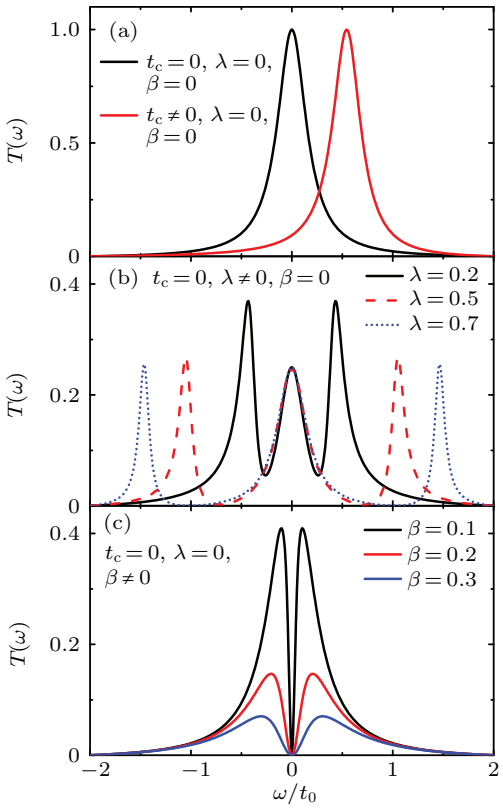


Fig. 2. Spectra of the transmission function of the double quantum dots influenced by interdot tunneling, Majorana tunneling or PT-symmetric complex potentials separately. The parameters used are (a) $t_c = 0.5$, (b) $\lambda = 0.2$, 0.5, 0.7, and (c) $\beta = 0.1$, 0.2, 0.3. All energies are measured in units of t_0.

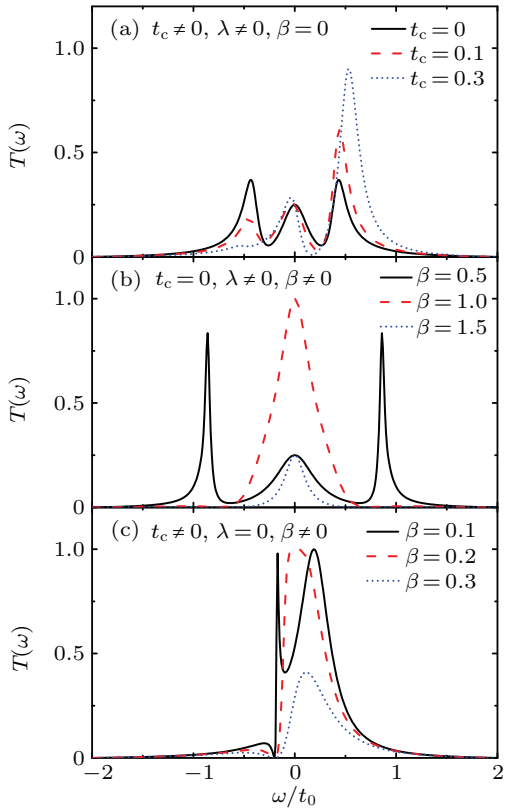


Fig. 3. Transmission function curves of the double quantum dots influenced by pairwise combination of interdot tunneling, Majorana tunneling and PT-symmetric complex potentials. The parameters used are (a) $\lambda = 0.2$ and $t_c = 0$, 0.1, 0.3, (b) $\lambda = 0.5$ and $\beta = 0.5$, 1, 1.5, $t_c = 0.2$ and (c) $\beta = 0.1$, 0.2, 0.3. All energies are measured in units of t_0.

Before we proceed, we plot the energy spectrum of the system to show the exceptional point. From Eq. (5), the real and imaginary parts of the eigenenergies are drawn in Fig. 4. In Figs. 4(a) and 4(b), it is seen that when $\beta < \sqrt{t_c^2 + (2\lambda)^2}$, the spectrum is real, while when $\beta > \sqrt{t_c^2 + (2\lambda)^2}$, the values of the energy are purely imaginary. At the special point $\beta = \sqrt{t_c^2 + (2\lambda)^2}$, which is the exceptional point, all of the energies collapse to zero. We define $\beta_{EP} = \sqrt{t_c^2 + (2\lambda)^2}$. The exceptional point appears at $t_c = \sqrt{\beta_{EP}^2 - (2\lambda)^2}$ in Figs. 4(c) and 4(d). In Fig. 5, we present the joint effects of β, λ and t_c. For $\beta < \beta_{EP}$, as seen in Fig. 5(a), the PT-symmetric complex potentials tune the two side peaks. With increasing β, these two side peaks approach each other. It is also seen that all of the curves in Fig. 5 are asymmetric around $\omega = 0$, which is induced by interdot coupling. When $\beta = \beta_{EP}$, i.e., at the exceptional point, the two side peaks merge and the transmission function reaches $T(\omega) = 1$, as seen in Fig. 5(b). When $\beta > \beta_{EP}$, the two side peaks disappear, and the $1/4$ central peak is restored, as seen in Fig. 5(c). In order to see the overall effects of λ, β and t_c, we plot a plane figure in Fig. 6. The exceptional point is located at $t_c = \sqrt{\beta_{EP}^2 - (2\lambda)^2} \approx 1.12$. For $t_c < \sqrt{\beta_{EP}^2 - (2\lambda)^2}$, there is a single $1/4$ peak. For $t_c > \sqrt{\beta_{EP}^2 - (2\lambda)^2}$, the transmission function shows the three-

peak structure. The interdot tunneling induces the asymmetry of the transmission function, which can be seen clearly in this figure.

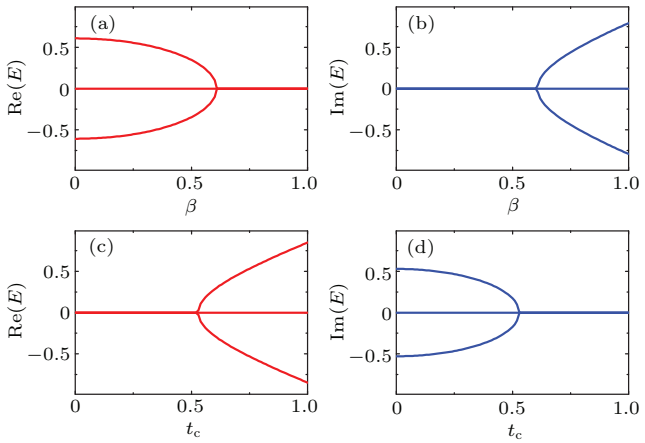


Fig. 4. Energy spectrum of the system. The real and imaginary parts are shown, as a function of PT-symmetric complex potentials in the upper row, and as a function of interdot tunneling in the lower row. The parameters used in (a) and (b) are $t_c = 0.1$ and $\lambda = 0.3$, while in (c) and (d) the parameters are $\beta = 0.8$ and $\lambda = 0.3$. All energies are measured in units of t_0.

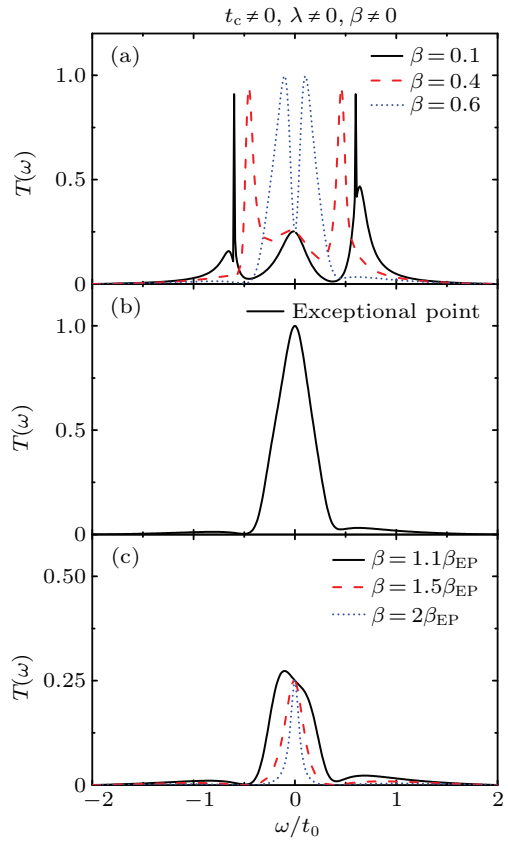


Fig. 5. Transmission function curves of the double quantum dots influenced by the interplay of interdot tunneling, Majorana tunneling and PT-symmetric complex potentials. The parameters used are $t_c = 0.1$ and $\lambda = 0.3$ in (a)–(c). The parameter used for PT-symmetric complex potentials is (a) $\beta = 0.1$, 0.4, 0.6, (b) $\beta = \beta_{EP}$, and (c) $\beta = 1.1\beta_{EP}, 1.5\beta_{EP}, 2\beta_{EP}$. All energies are measured in units of t_0.

Now we discuss the transport properties in the strong-coupling regime. We take dot–wire coupling as $v = 1$. The results are shown in Fig. 7. When the dot–wire coupling is strong, the window of resonant tunneling is broadened, and the transmission function shows a flat lineshape, as seen in Fig. 7. The effect of interdot tunneling remains, i.e., it still induces asymmetry in the transmission function. Interestingly, the participation of Majorana zero modes induces a $1/4$ conductance dip at $\omega = 0$, instead of the three-peak structure in the weak-coupling regime. When PT-symmetric complex potentials are added, they induce two side dips in the transmission function, which are located at $\omega = \pm\sqrt{t_c^2 + (2\lambda)^2} = \pm 0.5$. We notice that these two dips are pinned, no matter whether $\beta < \beta_{EP}$, $\beta = \beta_{EP}$ or $\beta > \beta_{EP}$, as seen in the curves of $\beta = 0.25$, 0.5 and 0.75 in Fig. 7(a). At the exceptional point $\beta = \sqrt{t_c^2 + (2\lambda)^2} = 0.5$, the central dip disappears, as seen in the curve of $\beta = 0.5$ in Fig. 7(a) or in the merging point at $\omega = 0$ and $\beta = 0.5$ in Fig. 7(b).

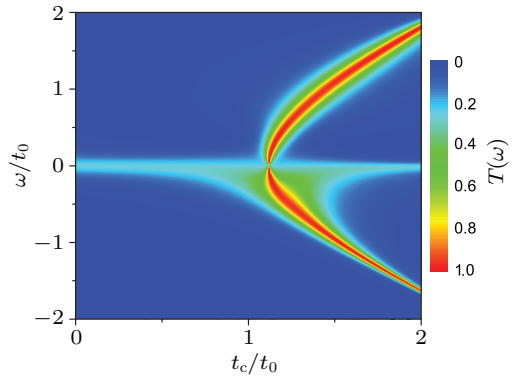


Fig. 6. Transmission coefficient as a function of ω and t_c. The parameter used are $v = 0.2$, $\beta = 1.5$, and $\lambda = 0.5$. All energies are measured in units of t_0.

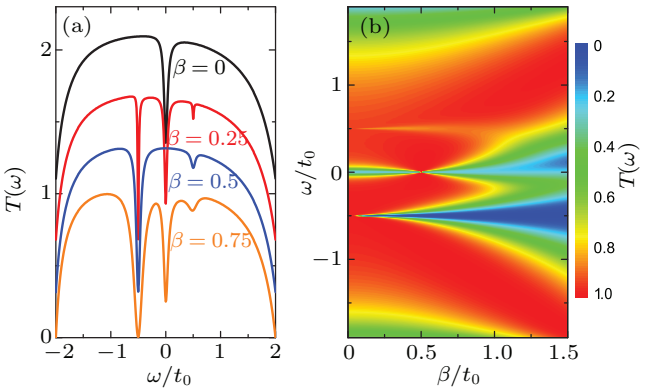


Fig. 7. Transmission function in the strong-coupling regime. In (a) and (b) the parameters used are $v = 1$, $t_c = 0.3$ and $\lambda = 0.2$. In (a) the values of PT-symmetric complex potentials are chosen as $\beta = 0$, 0.25, 0.5, 0.75. The curves for $\beta = 0$, 0.25, 0.5 are shifted upward for clarity. In (b) the value of β varies continuously. All energies are measured in units of t_0.

4. Conclusion

In summary, we have studied a model with a combination of non-Hermitian quantum dots and Majorana fermions. Some new effects were revealed in this quantum transport system. The interplay of PT-symmetric complex potentials, Majorana tunneling and interdot tunneling were investigated. By using the equation-of-motion technique, an analytical result for the retarded Green's functions has been obtained. It was

demonstrated that in the weak-coupling regime Majorana tunneling splits the single peak of the transmission function and maintains itself as a reduced $1/4$ conductance peak. The interdot tunneling only induces asymmetry, instead of moving the conductance peak, due to the robustness of Majorana modes. There is an exceptional point induced by the union of Majorana tunneling and interdot tunneling. With large enough PT-symmetric complex potentials and when the exceptional point is passed through, the three-peak structure of the transmission function is reduced to a single $1/4$ peak. In the strong-coupling regime, a Majorana fermion induces a $1/4$ conductance dip instead of the three-peak structure. PT-symmetric complex potentials induce two conductance dips pinned at the exceptional point. It was shown that this model generates some interesting results, which are accessible to experiments. These results may also be useful for the study of quantum transport models with gain and loss.

Acknowledgement

Project supported by the National Natural Science Foundation of China (Grant No. 11834005).

References

[1] Bender C M and Boettcher S 1998 *Phys. Rev. Lett.* **80** 5243
[2] Bender C M, *et al*. 2002 *Phys. Rev. Lett.* **89** 270401
[3] Bender C M 2007 *Rep. Prog. Phys.* **70** 947
[4] El-Ganainy R, *et al*. 2018 *Nat. Phys.* **14** 11
[5] Muller M and Rotter I 2008 *J. Phys. A: Math. Theor.* **41** 244018
[6] Moiseyev N 2011 *Non-Hermitian Quantum Mechanics* (Cambridge: Cambridge University Press)
[7] Ernzerhof M, *et al*. 2020 *J. Chem. Phys.* **152** 244119
[8] Rotter I 2009 *J. Phys. A: Math. Theor.* **42** 153001
[9] Malzard S, *et al*. 2015 *Phys. Rev. Lett.* **115** 200402
[10] Özdemir Ş K, *et al*. 2019 *Nat. Mater.* **18** 783
[11] Miri M A and Alù A 2019 *Science* **363** eaar7709
[12] Pikulin D I and Nazarov Y V 2013 *Phys. Rev. B* **87** 235421
[13] Hyart T and Lado J L 2022 *Phys. Rev. Research* **4** L012006
[14] Leijnse M and Flensberg K 2012 *Phys. Rev. B* **86** 134528
[15] Gong W J, *et al*. 2014 *Phys. Rev. B* **89** 245413
[16] Sherman D, *et al*. 2017 *Nat. Nanotechnol.* **12** 212
[17] Rančic M J, *et al*. 2019 *Phys. Rev. B* **99** 165306
[18] Cifuentes J D and Dias da Silva L G G V 2019 *Phys. Rev. B* **100** 085429
[19] Weymann I, *et al*. 2020 *Phys. Rev. B* **101** 235404
[20] Sanches J E, *et al*. 2020 *Phys. Rev. B* **102** 075128
[21] Majek P and Weymann I 2021 *Phys. Rev. B* **104** 085416
[22] Yang F B 2021 *Phys. Lett. A* **401** 127350
[23] Majek P, *et al*. 2022 *Phys. Rev. B* **106** 155123
[24] Majek P, *et al*. 2022 *Phys. Rev. B* **105** 075418
[25] Majek P and Weymann I 2022 *J. Mag. Mag. Mat.* **549** 168935
[26] Deng M X, *et al*. 2015 *Chin. Phys. B* **24** 037302
[27] Chen L, *et al*. 2018 *Chin. Phys. B* **27** 077102
[28] Albrecht S M, *et al*. 2016 *Nature* **531** 206
[29] Weymann I 2017 *J. Phys.: Condens. Matter* **29** 095301
[30] Majek P, *et al*. 2022 *Phys. Rev. B* **105** 075418
[31] Zhang L L and Gong W J 2017 *Phys. Rev. A* **95** 062123
[32] Zhang L L, *et al*. 2018 *Superlatt. Microstruct.* **113** 558
[33] Flensberg K 2010 *Phys. Rev. B* **82** 180516
[34] Liu D E and Baranger H U 2011 *Phys. Rev. B* **84** 201308
[35] Niu P B, *et al*. 2023 *Physica B* **663** 414974
[36] Zhang L L, *et al*. 2019 *Phys. Rev. A* **99** 032119
[37] Mourik V, *et al*. 2012 *Science* **336** 1003
[38] Flensberg K, von Oppen F and Stern A 2021 *Nature Rev. Mater.* **6** 944
[39] Meir Y and Wingreen N S 1992 *Phys. Rev. Lett.* **68** 2512
[40] Sun Q F, Guo H 2002 *Phys. Rev. B* **66** 155308
[41] Tolea M and Bulka B R 2007 *Phys. Rev. B* **75** 125301
[42] Liu Y, *et al*. 2006 *Phys. Lett. A* **360** 154
[43] Alvarez C, *et al*. 2015 *Phys. Lett. A* **379** 1062
[44] Haug H J W, Jauho A P 2008 *Quantum Kinetics in Transport and Optics of Semiconductors* (Berlin: Springer)
[45] Niu P B and Luo H G 2021 *Acta Phys. Sin.* **70** 117401 (in Chinese)